

Generation of all-to-all connections in a two-dimensional qubit array with two-body interactions

Tetsufumi Tanamoto¹

¹*Department of Information and Electronic Engineering,
Teikyo University, 1-1 Toyosatodai, Utsunomiya 320-8551, Japan*

All-to-all connections are required in general quantum annealing machines to solve various combinatorial optimization problems. The Lechner, Hauke, and Zoller (LHZ) method, which is used to realize the all-to-all connections, requires many-body interactions in locally connected qubits. Because most of the qubit interactions are two-body interactions, Lechner also proposed the construction of each four-body interaction by six controlled-NOT (CNOT) gates between two qubits. However, it is difficult to construct many CNOT gates. Herein, we show more concrete sequences to produce four-body and three-body interactions based on a two-dimensional solid-state qubit system. We show that the number of operations needed to construct the many-body interactions can be reduced using appropriate pulse sequences. These findings will help reduce quantum computation costs for solving combinatorial problems.

I. INTRODUCTION

The progress of artificial intelligence (AI) in science and technology is leading to significant changes in society. Faster solving of combinatorial optimization problems is a prerequisite condition for efficient development of AI algorithms such as deep-learning machine algorithms. The quantum annealing machine (QAM) is expected to efficiently solve the combinatorial optimization problems in a shorter time than is possible with classical annealing methods^{1–10}. Nishimori *et al.* developed the theoretical foundation of the QAM,^{1–3} and QAMs based on superconducting circuits are widely used^{11,12}. In a QAM, NP-hard problems, such as the traveling salesman problem, can be mapped to problems in finding the ground states of the Ising Hamiltonian, expressed by¹³ $H = \sum_{i<j} J_{ij} s_i^z s_j^z + \sum_i h_i s_i^z$, where the variable s_i^z is a classical bit of two values ($s_i^z = \pm 1$). The first term denotes the interaction, with a coupling constant J_{ij} , and the second term denotes the Zeeman energy with an applied magnetic field h_i . For a QAM, a tunneling term is added and the Hamiltonian is given by $H = \sum_{i<j} J_{ij} Z_i Z_j + \sum_i [h_i Z_i + \Delta_i(t) X_i]$, and the variables are expressed by Pauli matrices given by $X = \begin{pmatrix} 0 & 1 \\ 1 & 0 \end{pmatrix}$, and $Z = \begin{pmatrix} 1 & 0 \\ 0 & -1 \end{pmatrix}$. The tunneling term is controlled such that it disappears at the end of the calculation, given by $\Delta(t \rightarrow \infty) \rightarrow 0$. To solve many combinatorial problems, all connections between two cells are required. By contrast, interactions between solid-state qubits are limited to the nearest or next-nearest interactions. Choi introduced the minor embedding method to solve this problem in the D-Wave superconducting circuit structure.^{14,15} Lechner, Hauke, and Zoller (LHZ) proposed a novel method of realizing all connections by introducing a logical spin.¹⁶ Albash *et al.* compared the minor embedding and LHZ methods in terms of error tolerance and concluded that the minor embedding method is more error-tolerant than the LHZ method.¹⁷ However, the best method is decided according to the system, and

it is better that both methods should be equally investigated. Here we would like to investigate the LHZ method theoretically. One of the key challenges when using the LHZ method is to construct the four-body interactions. Kerr nonlinearity based on Josephson parametric oscillators is one of the promising candidates proposed for realizing the LHZ scheme.^{18–21} As the two-photon drive strength increases, the system enters a stable cat state as the result of the bifurcation. However, the Kerr effect can be observed in some limited systems. Lechner also proposed the construction method of using controlled-NOT (CNOT) gates. He showed that the number of the CNOT gates required for constructing a single four-qubit interaction is six. However, in general, the CNOT gates are complicated to build, and it is difficult to use many CNOT gates for constructing the quantum annealing process. Herein, we propose a method that enables every qubit system interacting with nearest-neighbor Ising interactions to realize the LHZ Hamiltonian. We dynamically form the many-body interactions by using appropriate pulse sequences.

We propose a more concrete method to construct the four-qubit interactions without directly using the CNOT gates. It is shown that the dynamic pulse sequences by single-qubit rotations and two-body interactions enable the formation of the four-body and three-body interactions.

The rest of this paper is organized as follows. In Section II, we show our dynamical pulse sequence using the effective Hamiltonian method in²². In Section III, we show the numerical results of the success probability of our method. In Section IV, we discuss our results. In Section V, we summarize and conclude this study.

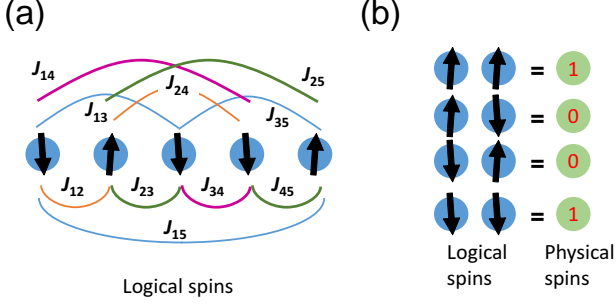


FIG. 1: LHZ scheme for generating the all-to-all connections.¹⁶ (a) Ten connections exist for five logical spins. (b) In LHZ,¹⁶ one physical qubit represents two physical spins such that two parallel spins correspond to qubit "0" and two antiparallel spins correspond to qubit "1."

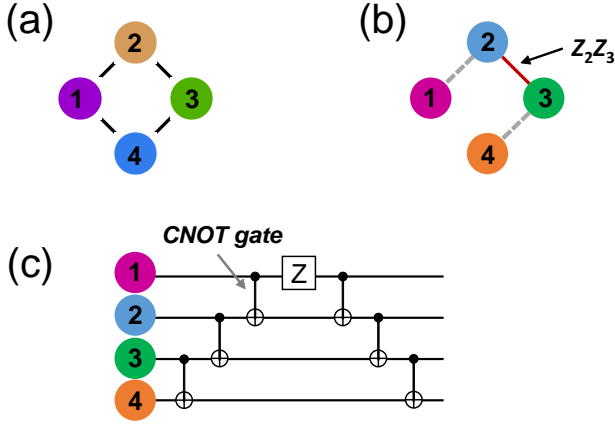


FIG. 2: (a) Four-body interaction $Z_1Z_2Z_3Z_4$ in LHZ. (b) Realization of the four-body interaction by two-body interactions J_{12}, J_{13} , and J_{34} . The solid brown line shows an initial Hamiltonian that uses Eq. (8). The dotted lines show the required interactions to form the four-body interaction. (c) Lechner's method to construct the four-body interaction.²³

II. EFFECTIVE HAMILTONIAN METHOD

A. Previously proposed method for constructing many-body interactions

In the LHZ method, the all-to-all connections shown in Fig. 1(a) are realized by the replacement of Fig. 1(b).¹⁶ The key point is to introduce the four-body interaction into the Hamiltonian described by

$$H^{\text{LHZ}} = \sum_i [A(t_a)X_i + B(t_a)J_iZ_i] - \lambda \sum_i Z_{C_u^{(i)}} Z_{C_d^{(i)}} Z_{C_l^{(i)}} Z_{C_r^{(i)}}, \quad (1)$$

where $A = 1$ and $B = 0$ at $t_a = 0$ and $A = 0$ and $B = 1$ at the end of the calculation. $C_c^{(i)}, \{c \in u, d, l, r\}$ are

the neighboring qubits of qubit i . The four-body interaction represents the constraint of Fig. 1(b), which means that the physical spin states consist of an even number of spins. At the boundary sites, this four-body interaction changes to three-body interaction. Lechner also used the quantum approximate optimization algorithm (QAOA) scheme, in which the Hamiltonian $H_0 + H_{\text{int}}$ is separated into components of the single-qubit rotations H_0 and the interaction parts H_{int} .^{23,24} The rotation angles of the single qubits and the interactions are determined by a feedback loop of measuring the outcome of the previous measurements. Once the interaction part $\lambda \sum_i Z_{C_u^{(i)}} Z_{C_d^{(i)}} Z_{C_l^{(i)}} Z_{C_r^{(i)}}$ is separated, this part is constructed by a series of qubit operations.

Let us estimate the number of processes required to construct the four-body interactions proposed by Lechner.²³ For the Ising Hamiltonian $H_{\text{int}} = \sum_{i<j} J_{ij}Z_iZ_j$, the conditional phase flip (CPF) gate is given by $R_1^z(\theta_4)R_2^z(\theta_4)e^{i\theta_4Z_1Z_2}$, where $\theta_4 \equiv \pi/4$, and $R_i^\alpha(\theta) \equiv \exp\{i\theta\alpha_i\}$ is a single-qubit rotation. The CNOT gate between qubits 1 and 2 is given by $U_{12}^{\text{CNOT}} = R_2^y(-\theta_4)U_{12}^{\text{CPF}}R_2^y(\theta_4)$, and the time to obtain the CNOT gate is given by $\tau_{\text{CNOT}} \approx 4\tau_{\text{rot}} + \tau_J$, where τ_{rot} represents the time of the single-qubit rotation and $\tau_J = \pi/(4J)$. Then, the time required to obtain the conditions in Fig. 2(c) is given by $25\tau_{\text{rot}} + 6\tau_J$. For the XY model,²⁶ the CNOT gate is expressed by

$$U_{12}^{\text{CNOT}} = R_1^z(-\theta_4)R_2^x(\theta_4)R_2^z(\theta_4)U_{12}^{\text{iSWAP}}R_1^x(\theta_4) \times U_{12}^{\text{iSWAP}}R_2^z(\theta_4) \quad (2)$$

where $U_{12}^{\text{iSWAP}} \equiv \exp\{i\theta_4[X_1X_2 + Y_1Y_2]\}$. Thus, we have $\tau_{\text{CNOT}} \approx 4\tau_{\text{rot}} + 2\tau_J$, and the time required to obtain the conditions in Fig. 2(c) is given by $25\tau_{\text{rot}} + 12\tau_J$. Thus a lot of qubit operations are required to construct a single four-body interaction.

B. A creation of the four-body interaction using the effective Hamiltonian method

Here, we show our scheme for creating the effective Hamiltonian of Eq. (1). In order to see the true effect of our method, we do not use the feedback of the QAOA approach, and we simply approximate the time evolution of the total Hamiltonian into small intervals of time. A given time t is separated into smaller pieces $t = \sum_{i=0}^{N_a} \Delta t$ with $\Delta t = t/N_a$ with an integer N_a . Thus, in our method, the time evolution is expressed by

$$U(t) = \prod_{l=1}^{N_a} U_{\text{unit}}(t_l, t_{l-1}) \quad (3)$$

where $t_{N_a} = t$ and $t_0 = 0$, and $t_l - t_{l-1} = \tau_{sq} + \tau_{mb}$.

$$U_{\text{unit}}(t_l, t_{l-1}) \approx e^{-i\tau_{sq} \sum_i [A(t_i)X_i + B(t_i)h_iZ_i]} \times e^{-iJ\tau_{mb} \sum_i Z_iZ_jZ_kZ_l}. \quad (4)$$

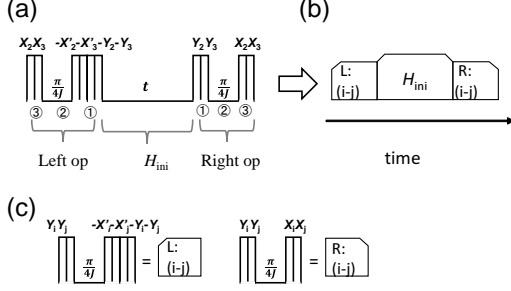


FIG. 3: (a) Basic pulse sequence to produce the four-body interaction from the initial Hamiltonian $H_{\text{ini}} = Z_2 Z_3$. (b) Graphical description of the formation of the four-body interaction using the pulse element of (c); see Eq. (10).

By using the Baker-Campbell-Hausdorff(BCH) formula $e^{H_1} e^{H_2} = e^{H_3}$, where $H_3 = H_1 + H_2 + [H_1, H_2]/2 + [H_1, [H_1, H_2]]/12 - [H_2, [H_1, H_2]]/12..$, we neglect the commutation relations $[H_1, H_2]$. In our method, the magnitude of the constraint term is adjusted by the time period of τ_{mb} . Once the unitary evolution is separated into each component, we can multiply those unitary operations directly one-by-one, and we can construct many-body interactions starting from two-body interactions. Here we focus on the case of the Ising interaction, and we consider the conversion of the two-body interaction $\sum_{i,j} J_{ij} Z_i Z_j$ into the four-body interaction $\sum_{i,j,k,l} J_{ijkl} Z_i Z_j Z_k Z_l$. The core idea is to apply the effective Hamiltonian method²² to the Hamiltonian $H_{\text{eff}} = \sum Z_i Z_j Z_k Z_l$. The effective Hamiltonian H_{eff} is produced from its initial form H_{ini} by applying a series of operations H_j^{op} such that

$$H_{\text{eff}} \rightarrow \prod_{j=1}^n \exp(-i\tau_j^{\text{op}} H_j^{\text{op}}) H_{\text{ini}} \prod_{j=n}^1 \exp(i\tau_j^{\text{op}} H_j^{\text{op}}). \quad (5)$$

The increase in the degree of the many-body interactions is carried out by the basic equations:²²

$$e^{-i\theta Z_1 Z_2} X_1 e^{i\theta Z_1 Z_2} = \cos(2\theta) X_1 + \sin(2\theta) Y_1 Z_2, \quad (6)$$

$$e^{-i\theta Z_1 Z_2} Y_1 e^{i\theta Z_1 Z_2} = \cos(2\theta) Y_1 - \sin(2\theta) X_1 Z_2. \quad (7)$$

For example, if we apply the pulse during $\theta = J\tau_J$, we obtain

$$Y_1 \rightarrow X_1 Z_2. \quad (8)$$

Repetitions of these equations enable the transformation of m -body interactions into $(m+1)$ -body interactions.

As a simple example, we consider the construction of a single four-body interaction including four spins (Fig. 2). We assume that there is a mechanism for switching interactions on and off. The initial Hamiltonian is given by $H_{\text{ini}} = JZ_2 Z_3$, where other interactions $Z_1 Z_2$, $Z_3 Z_4$, and $Z_4 Z_1$ are initially switched off. Once we prepare $H_{\text{ini}} = JZ_2 Z_3$, we can change this Hamiltonian by three

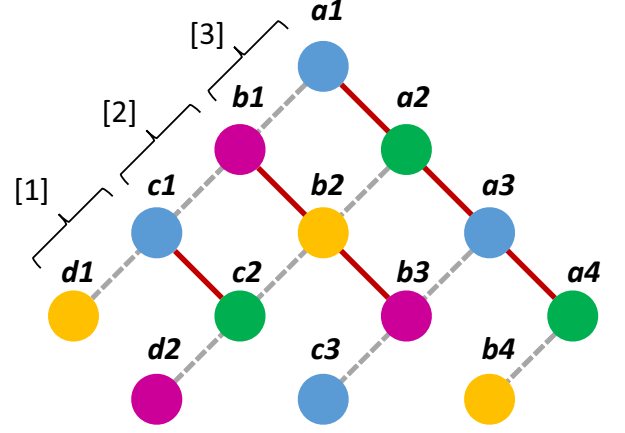


FIG. 4: Distribution of interactions to realize all-to-all connections for six logical qubits by forming the four-body interactions; an application of our method to the LHZ scheme. Bold lines show the interactions of the initial Hamiltonian H_{ini} . Dotted lines show the interactions to be formed from the pulse sequence. Ising interactions are assumed to be switched on and off between the qubits.

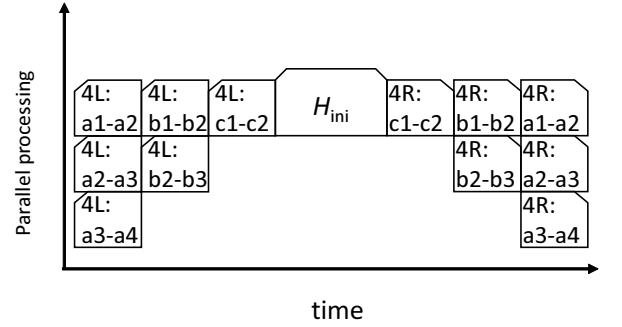


FIG. 5: Graphical description of the generation of four-body interaction in the 13-qubit system shown in Fig. 4. Parallel processing is possible; see Eq. (12).

steps given by

$$\begin{aligned} H_{\text{int}} &= JZ_2 Z_3 \Rightarrow JX_2 X_3 \quad : [\text{step1}] \\ &\Rightarrow J(Y_2 Z_1)(Y_3 Z_4) \quad : [\text{step2}] \\ &\Rightarrow JZ_1 Z_2 Z_3 Z_4 \quad : [\text{step3}] \end{aligned} \quad (9)$$

Here, in step 1, we apply a $\pi/2$ pulse around the y -axis, given by $e^{-i(\pi/4)Y_i} Z_i e^{i(\pi/4)Y_i} = X_i$ for qubits 2 and 3. In step 2, free running of the system during the period of $\pi/(4J)$ leads to the use of Eq. (8). In step 3, we apply a $\pi/2$ pulse around the x -axis such that $e^{i(\pi/4)X_i} Z_i e^{-i(\pi/4)X_i} = Y_i$ for qubits 2 and 3. These processes are described in Fig. 3.

$$\begin{aligned} &R_{2,3}^X(-\theta_4) [R_{2,3}^X(2\theta_4) e^{-i\tau_J [Z_1 Z_2 + Z_3 Z_4]} R_{2,3}^X(-2\theta_4)] \\ &\times R_{2,3}^Y(-\theta_4) e^{-itZ_2 Z_3} R_{2,3}^Y(\theta_4) e^{-i\tau_J [Z_1 Z_2 + Z_3 Z_4]} R_{2,3}^X(\theta_4), \end{aligned} \quad (10)$$

where $R_{2,3}^\alpha(\theta) = \exp(i\theta[\alpha_2 + \alpha_3])$ ($\alpha = X, Y$). The square bracket is required to change $e^{-i\tau_J[Z_1 Z_2 + Z_3 Z_4]}$ into $e^{i\tau_J[Z_1 Z_2 + Z_3 Z_4]}$, and we can reduce $R_{2,3}^X(-\theta_4)R_{2,3}^X(2\theta_4) = R_{2,3}^X(\theta_4)$ in the first line of the equation. Thus, the required time is $5\tau_{\text{rot}} + 2\tau_J$, which is 1/6 times less than that of Lechner's method.

The general case is the repetition of the single-four qubit case. Figure 4 shows the order of the operations for 13 qubits. The initial Hamiltonian is given by

$$H_{\text{ini}} = Z_{a1}Z_{a2} + Z_{a2}Z_{a3} + Z_{a3}Z_{a4} \\ + Z_{b1}Z_{b2} + Z_{b2}Z_{b3} + Z_{c1}Z_{c2}. \quad (11)$$

We start from block [1], and blocks [2] and [3] are followed serially. The detailed pulse sequence of the 13 qubits is given by the following, where the bold characters show the operations at each step:

$$\begin{aligned} H_{\text{ini}} &\Rightarrow Z_{a1}Z_{a2} + Z_{a2}Z_{a3} + Z_{a3}Z_{a4} \\ &+ Z_{b1}Z_{b2} + Z_{b2}Z_{b3} + \mathbf{X}_{c1}\mathbf{X}_{c2} : [\text{step1}] \\ &\Rightarrow Z_{a1}Z_{a2} + Z_{a2}Z_{a3} + Z_{a3}Z_{a4} \\ &+ Z_{b1}Z_{b2} + Z_{b2}Z_{b3} + \mathbf{Y}_{c1}\mathbf{Z}_{d1}\mathbf{Y}_{c2}\mathbf{Z}_{d2} : [\text{step2}] \\ &\Rightarrow Z_{a1}Z_{a2} + Z_{a2}Z_{a3} + Z_{a3}Z_{a4} \\ &+ \mathbf{X}_{b1}\mathbf{X}_{b2} + \mathbf{X}_{b2}\mathbf{X}_{b3} + Z_{c1}Z_{d1}Z_{c1}Z_{d2} : [\text{step3}] \\ &\Rightarrow Z_{a1}Z_{a2} + Z_{a2}Z_{a3} + Z_{a3}Z_{a4} \\ &+ \mathbf{Y}_{b1}\mathbf{Z}_{c1}\mathbf{Y}_{b2}\mathbf{Z}_{c2} + \mathbf{Y}_{b2}\mathbf{Z}_{c2}\mathbf{Y}_{b3}\mathbf{Z}_{c3} + Z_{c1}Z_{d1}Z_{c1}Z_{d2} : [\text{step4}] \\ &\Rightarrow \mathbf{X}_{a1}\mathbf{X}_{a2} + \mathbf{X}_{a2}\mathbf{X}_{a3} + \mathbf{X}_{a3}\mathbf{X}_{a4} \\ &+ Z_{b1}Z_{c1}Z_{b2}Z_{c2} + Z_{b2}Z_{c2}Z_{b3}Z_{c3} + Z_{c1}Z_{d1}Z_{c1}Z_{d2} : [\text{step5}] \\ &\Rightarrow \mathbf{Y}_{a1}\mathbf{Z}_{b1}\mathbf{Y}_{a2}\mathbf{Z}_{b2} + \mathbf{Y}_{a2}\mathbf{Z}_{b2}\mathbf{Y}_{a3}\mathbf{Z}_{b3} + \mathbf{Y}_{a3}\mathbf{Z}_{b3}\mathbf{Y}_{a4}\mathbf{Z}_{b4} \\ &+ Z_{b1}Z_{c1}Z_{b2}Z_{c2} + Z_{b2}Z_{c2}Z_{b3}Z_{c3} + Z_{c1}Z_{d1}Z_{c1}Z_{d2} : [\text{step6}] \\ &\Rightarrow \mathbf{Z}_{a1}\mathbf{Z}_{b1}\mathbf{Z}_{a2}\mathbf{Z}_{b2} + \mathbf{Z}_{a2}\mathbf{Z}_{b2}\mathbf{Z}_{a3}\mathbf{Z}_{b3} + \mathbf{Z}_{a3}\mathbf{Z}_{b3}\mathbf{Z}_{a4}\mathbf{Z}_{b4} \\ &+ Z_{b1}Z_{c1}Z_{b2}Z_{c2} + Z_{b2}Z_{c2}Z_{b3}Z_{c3} + Z_{c1}Z_{d1}Z_{c1}Z_{d2} : [\text{step7}] \end{aligned} \quad (12)$$

Note that the process of $Y_i Z_j \rightarrow Z_i Z_j$, which is the third step in Eq. (9), can overlap the next four-body generation step. Thus, for the three blocks ($N_b = 3$), we have $2 \times 2 + 3 = 7$ steps of operations.

These processes are easily extended to a general case. The addition of one block line adds two steps. As shown in Fig. 4, the $[N_b]$ -th block includes N_b squares and N_b four-qubit interactions. Thus, the $[N_b]$ block system includes $(N_b + 1)(N_b + 2)/2 + N_b$ qubits and $N_b(N_b + 1)/2$ initial interactions by $2N_b + 1$ steps. The number of logical qubits, $N_b(N_b + 1)/2$ interactions, is feasible. The generation time is estimated from the graphical description of Fig. 5. The right part includes a time of $N_b(\tau_J + \tau_{\text{rot}}) + \tau_{\text{rot}}$, and the left part includes a time of $N_b(\tau_J + 2\tau_{\text{rot}}) + \tau_{\text{rot}}$. Thus, we need a total time of $N_b(2\tau_J + 3\tau_{\text{rot}}) + 2\tau_{\text{rot}}$ by using parallel processing (Fig. 4).

C. Creation of the three-body interaction

As Lechner^{16,25} derived, the LHZ condition is also satisfied by a three-qubit interaction using ancilla qubits. The replacement of the four-body interaction by the three-body interaction is expressed by²⁵

$$Z_1 Z_2 Z_3 Z_4 \rightarrow Z_1 Z_2 Z_a + Z_3 Z_4 Z_a, \quad (13)$$

where Z_a is the element of the ancilla qubit. It can be shown that the three-body interaction is derived from the two-body interactions similarly to the four-body interaction mentioned above. Figure 6 shows the formation process of three blocks, where six ancilla qubits (p_i, q_i, r_i) are prepared. The initial Hamiltonian is given by

$$\begin{aligned} H_{\text{ini}} &= Z_{a1}Z_{p1} + Z_{a2}Z_{p2} + Z_{a3}Z_{p3} \\ &+ Z_{b1}Z_{p1} + Z_{b2}Z_{p2} + Z_{b3}Z_{p3} \\ &+ Z_{b1}Z_{q1} + Z_{b2}Z_{q2} + Z_{c1}Z_{q1} + Z_{c2}Z_{q2} \\ &+ Z_{c1}Z_{r1} + Z_{d1}Z_{r1}. \end{aligned} \quad (14)$$

We start from block [1], which includes the line with the smallest number of qubits. The transformation of the Hamiltonian is carried out stepwise by using Eqs. (6) and (7), similar to the four-body interaction. The number of steps is the same as that of the four-body interaction (see Appendix B). The graphical description of the three-body generation is shown in Fig. 7. The generation time is the same as that of the four-body interaction and is given by $N_b(2\tau_J + 3\tau_{\text{rot}}) + 2\tau_{\text{rot}}$. The difference between the four-body generation and the three-body interaction is that the qubits that are controlled are mutually separated in the three-body generation case because of the existence of the ancilla qubits. This will be helpful in fabricating the gate electrodes to control the qubits. The disadvantage of the three-body interaction array is that the number of qubits is larger than that of the four-body interaction case.

III. NUMERICAL CALCULATION

We calculate the success probability of our method for the four-body interaction in six qubits. The time evolution of the unitary matrix is calculated using the Chebyshev expansion,²⁷ and overlapping the evolution with the exact wave functions is estimated. The initial input data h_i are randomly chosen ($i = 1, \dots, 6$). The limited number of qubits is caused by the calculation resources. For this reason, the number of qubits (six qubits) in the three-body interaction is not calculated here.

The three types of the annealing schedules considered for $A(t_a) = \Delta(t_a)$ and $B(t_a) = 1 - \Delta(t_a)$ in Eq. (1) are given by

$$\begin{aligned} \Delta(t_a) &= 1 - t_a, \quad (\text{I}) \\ \Delta(t_a) &= 1 - \exp(-t_a), \quad (\text{II}) \\ \Delta(t_a) &= 1/\sqrt{t_a + 1}. \quad (\text{III}) \end{aligned}$$

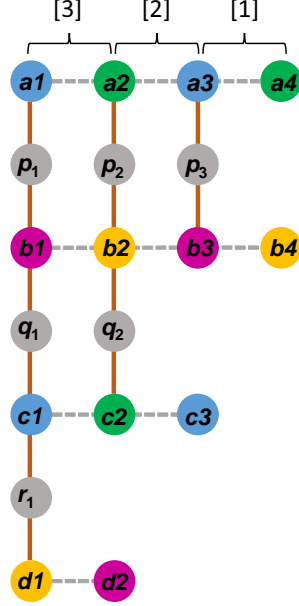


FIG. 6: An application of our method to the LHZ scheme of three-body interactions. The distribution of interactions realizes all-to-all connections for six logical qubits by three-body interactions. Bold lines show the interactions of the initial Hamiltonian H_{ini} . Dotted lines show the interactions to be created from the pulse sequence. The three-body interactions are generated by three blocks. In the first block [1], the three-body interaction regarding the rightmost line is generated. In the second block [2], the three-body interaction regarding the middle line is generated; in the third block [3], the three-body interaction regarding the left line is generated. In total, a seven-pulse sequence is required. The extension to more qubits is straightforward.

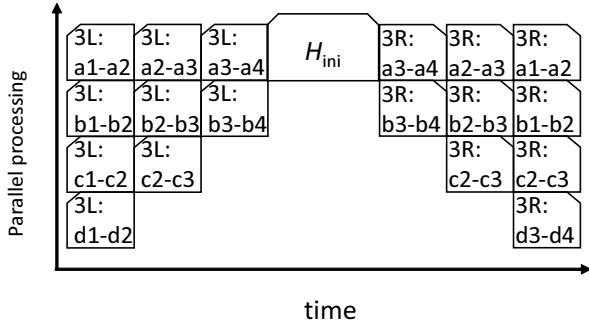


FIG. 7: Graphical description of the generation of the three-body interaction of Fig. 6. Parallel processing is possible; see Eq. (B1).

In this calculation, $A = 1$ and $B = 0$ at $t_a = 0$ and $A = 0$ and $B = 1$ at $t_a = 1$. The time $0 < t_a < 1$ is divided into N_a steps, during each of which the single unit of Eq. (4) is carried out.

In order to use the BCH formula in Eq.(3), the time step t_a/N_a should be sufficiently small. When we follow

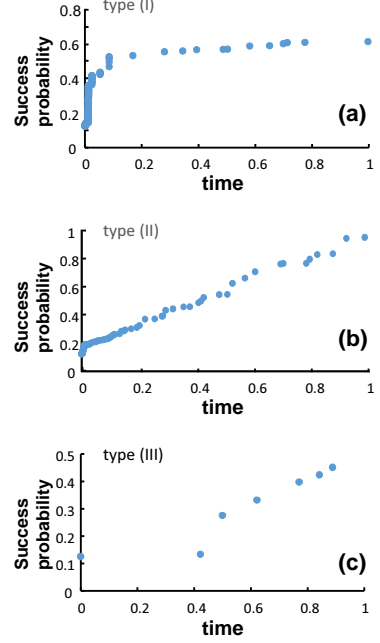


FIG. 8: Numerically calculated success probability of the annealing process. (a) $\Delta(t_a) = 1 - t_a$, (b) $\Delta(t_a) = 1 - \exp(-t_a)$, and (c) $\Delta(t_a) = 1/\sqrt{t_a + 1}$. $\tau_{sb} = \pi/200$, $N_S = 50$ and $J\tau_M = \pi/2$. The annealing time t_a is divided into $N = 10^5$ steps. Each time step has a time interval of $\tau_S + \tau_M$ as shown in Eq. (4) where $\tau_S = N_S\tau_{sq}$. Thus, the real elapsed time is estimated by $N(\tau_S + \tau_M)$.

the calculational procedure of Eq.(3), we have to calculate many sets of $U_{\text{unit}}(t_l, t_{l-1})$. In this procedure, the N_a times of the formation of the many-body interactions is repeated, and the operations complexity increases as the time step t_a/N_a becomes smaller. It is found that the success probabilities does not reach one in the calculations of the range $N_a \sim 10^6$ (figures not shown). Thus, we think that, if the time step is sufficiently small, we can rearrange the order of the operations Eq.(3) such as

$$U(t_l, t_{l-1})U(t_{l+1}, t_l) \approx e^{-i\tau_{sq}H^{\text{SQ}}(t_l)}e^{-i\tau_{sq}H^{\text{SQ}}(t_{l+1})} \times e^{-i2\tau_{mb}H^{\text{MB}}}, \quad (15)$$

where $H^{\text{SQ}}(t_l) \equiv \sum_i [A(t_l)X_i + B(t_l)h_iZ_i]$ and $H^{\text{MB}} \equiv J \sum Z_i Z_j Z_k Z_l$. Then we can collect parts of Eq.(3), and the whole unitary operations consist of the lumps of smaller processes each of which has N_S times of H^{SQ} and H^{MB} . That is, one lump contains $\prod_{i=l'}^{l'+N_S} e^{-i\tau_{sq}H^{\text{SQ}}(t_i)}$ and $e^{-iN_S\tau_{mb}H^{\text{MB}}}$. This method has the advantage of maximizing the effect of the constraints of the four-body interaction, for $J\tau_M = \pi/2 + m\pi$ with integer m where $\tau_M \equiv N_S\tau_{mb}$, because of the relationship $e^{-i\tau_M H^{\text{MB}}} = \cos(J\tau_M) - i \sin(J\tau_M)H^{\text{MB}}/J$. Hereafter, we treat this method to estimate the success probabilities.

Figure 8 shows the result of $N = 10^5$ and $N_S = 50$. It is found that type (II) is the best for scheduling. As N and N_S become larger, the success probability increases.

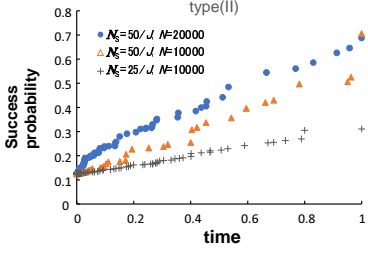


FIG. 9: Numerically calculated success probability of the annealing process of type (II) ($\Delta(t_a) = 1 - \exp(-t_a)$) when the N and N_S are reduced.

Next we consider whether N can be reduced or not by focusing on the type (II). Figure 9 shows different parameter regions of N and N_S for the type (II). It is found that the reduction of N_S degrades the success probability. Although the N in Fig. 9 is about one-fifth smaller than the N in Fig. 8, the success probability of Fig. 9 become about 80% of Fig. 8. These results show that the speed to reach to the maximum success probability becomes slower when the success probability become close to one. From the realistic viewpoint, the stopping point of the annealing process will depend on the requirement of the accuracy of the individual solution.

IV. DISCUSSIONS

We estimate the time required to carry out our processes regarding the calculations of Fig. 8. When we choose $J = 100\mu\text{eV}$ assuming $\tau_{\text{rot}} \ll \tau_J$ and $N_b = 3$, we have $J\tau_M = 6\tau_{\text{rot}} + 11\pi/2 \sim 11\pi/2$, and $\tau_M \sim 7.15 \times 10^{-10}\text{s}$. For $N_S = 50$, we have $\tau_S \sim 4.14 \times 10^{-8}\text{s}$. The repetition of $\tau_M + \tau_S$ by $N = 10^5$ times leads to 278 μs as the total annealing time. Because the operation times are limited by the coherence time of the system, we have to reduce the annealing time. In order to reduce the total annealing time, we must increase the strength of the coupling J . If we apply our idea to a quantum annealing machine based on floating gates (FG)^{28,29} with 15 nm width, 100 nm height, and tunneling oxide thickness 3.5 nm, we have $J \approx 10.34$ meV and $\tau_J \approx 0.304$ ps. Then, we have the total annealing time of 2.69 μs . As J increases, the number of qubits could be increased. Whether the feedback developed in the QAOA²⁴ is effective to optimize the number of the annealing process of our model is a future problem.

V. CONCLUSIONS

In this study, we proposed a method to construct four-qubit interactions without directly using CNOT gates in QAMs. We considered concrete pulse sequences for the all-to-all connection of the LHZ method.¹⁶ We applied the effective Hamiltonian theory²² and showed that

the form of the four-body interaction can be constructed without directly using CNOT gates. The processes for generating the four-body interaction and the three-body interaction have the same number of steps. As the number of steps increases, the success probability increases. The total annealing time is determined by the size of the system and the coherence time. The findings of this study will help reduce computation costs for solving combinatorial problems in quantum annealing. We treated the simple case of no feedback in the process of obtaining optimal annealing parameters. In future work, it should be discussed whether the number of steps can be reduced using the feedback loop as in the QAOA methods.

Acknowledgments

We are grateful to T. Mori, H. Fuketa, J. Deguchi, Y. Nishi, and H. Goto for the fruitful discussions. This work was partly supported by MEXT Quantum Leap Flagship Program (MEXT Q-LEAP) Grant Number JP-MXS0118069228, Japan.

Appendix A: Basic formula

The operations treated here are derived from the fundamental mathematical equations. The single-qubit rotation is given by

$$\exp(-i\theta\sigma^\alpha)\sigma^\beta\exp(i\theta\sigma^\alpha) = \cos(2\theta)\sigma^\beta + \epsilon_{\alpha\beta\gamma}\sin(2\theta)\sigma^\gamma \quad (\text{A1})$$

where $\epsilon_{\alpha\beta\gamma}$ is the Levi-Civita symbol ($\{\alpha, \beta, \gamma\} = \{x, y, z\}$), and σ_α are the Pauli matrices. These equations are derived by the relationship $e(i\theta\sigma^\alpha) = \cos\theta + i\sigma_\alpha\sin\theta$.

Appendix B: Steps in the three-body interaction

The detailed pulse sequence for generating the three-body interactions in Fig. 6 is given by the following (bold

characters show the operations at each step):

$$\begin{aligned}
H_{\text{ini}} &\Rightarrow Z_{a1}Z_{p1} + Z_{a2}Z_{p2} + \mathbf{X}_{a3}Z_{p3} \\
&+ Z_{b1}Z_{p1} + Z_{b2}Z_{p2} + \mathbf{X}_{b3}Z_{p3} + \dots : [\text{step1}] \\
&\Rightarrow Z_{a1}Z_{p1} + Z_{a2}Z_{p2} + \mathbf{Y}_{a3}\mathbf{Z}_{a4}Z_{p3} \\
&+ Z_{b1}Z_{p1} + Z_{b2}Z_{p2} + \mathbf{Y}_{b3}\mathbf{Z}_{b4}Z_{p3} + \dots : [\text{step2}] \\
&\Rightarrow Z_{a1}Z_{p1} + \mathbf{X}_{a2}Z_{p2} + Y_{a3}Z_{a4}Z_{p3} \\
&+ Z_{b1}Z_{p1} + \mathbf{X}_{b2}Z_{p2} + Y_{b3}Z_{b4}Z_{p3} \\
&+ Z_{b1}Z_{q1} + \mathbf{X}_{b2}Z_{q2} + Z_{c1}Z_{q1} + \mathbf{X}_{c2}Z_{q2} + \dots : [\text{step3}] \\
&\Rightarrow Z_{a1}Z_{p1} + \mathbf{Y}_{a2}\mathbf{Z}_{a3}Z_{p2} + \mathbf{Z}_{a3}Z_{a4}Z_{p3} \\
&+ Z_{b1}Z_{p1} + \mathbf{Y}_{b2}\mathbf{Z}_{b3}Z_{p2} + \mathbf{Z}_{b3}Z_{b4}Z_{p3} \\
&+ Z_{b1}Z_{q1} + \mathbf{Y}_{b2}\mathbf{Z}_{b3}Z_{q2} + Z_{c1}Z_{q1} + \mathbf{Y}_{c2}\mathbf{Z}_{c3}Z_{q2} + \dots : [\text{step4}] \\
&\Rightarrow \mathbf{X}_{a1}Z_{p1} + Y_{a2}Z_{a3}Z_{p2} + Z_{a3}Z_{a4}Z_{p3} \\
&+ \mathbf{X}_{b1}Z_{p1} + Y_{b2}Z_{b3}Z_{p2} + Z_{b3}Z_{b4}Z_{p3} \\
&+ \mathbf{X}_{b1}Z_{q1} + Y_{b2}Z_{b3}Z_{q2} + \mathbf{X}_{c1}Z_{q1} + Y_{c2}Z_{c3}Z_{q2} \\
&+ \mathbf{X}_{c1}Z_{r1} + \mathbf{X}_{d1}Z_{r1} : [\text{step5}] \\
&\Rightarrow \mathbf{Y}_{a1}\mathbf{Z}_{a2}Z_{p1} + Z_{a2}Z_{a3}Z_{p2} + Z_{a3}Z_{a4}Z_{p3} \\
&+ \mathbf{Y}_{b1}\mathbf{Z}_{b2}Z_{p1} + Z_{b2}Z_{b3}Z_{p2} + Z_{b3}Z_{b4}Z_{p3} \\
&+ \mathbf{Y}_{b1}\mathbf{Z}_{b2}Z_{q1} + Z_{b2}Z_{b3}Z_{q2} + Y_{c1}Z_{c2}Z_{q1} + Z_{c2}Z_{c3}Z_{q2} \\
&+ \mathbf{Y}_{c1}\mathbf{Z}_{c2}Z_{r1} + \mathbf{Y}_{d1}\mathbf{Z}_{d2}Z_{r1} : [\text{step6}] \\
&\Rightarrow \mathbf{Z}_{a1}Z_{a2}Z_{p1} + Z_{a2}Z_{a3}Z_{p2} + Z_{a3}Z_{a4}Z_{p3} \\
&+ \mathbf{Z}_{b1}Z_{b2}Z_{p1} + Z_{b2}Z_{b3}Z_{p2} + Z_{b3}Z_{b4}Z_{p3} \\
&+ \mathbf{Z}_{b1}Z_{b2}Z_{q1} + Z_{b2}Z_{b3}Z_{q2} + Z_{c1}Z_{c2}Z_{q1} + Z_{c2}Z_{c3}Z_{q2} \\
&+ \mathbf{Z}_{c1}Z_{c2}Z_{r1} + \mathbf{Z}_{d1}Z_{d2}Z_{r1} : [\text{step7}]
\end{aligned} \tag{B1}$$

-
- ¹ T. Kadowaki and H. Nishimori, Phys. Rev. E **58**, 5355(1998).
² S. Morita and H. Nishimori, J. Math. Phys. **49**, 125210 (2008).
³ E. Farhi, J. Goldstone, S. Gutmann, J. Lapan, A. Lundgren, and D. Preda, Science **292**, 472 (2001).
⁴ R. Barends, *et al.*, Nature **534**, 222 (2016).
⁵ S. J. Weber, *et al.*, Phys. Rev. Applied **8**, 014004 (2017).
⁶ M. Ohzeki, J. Phys. Soc. Jpn. **88**, 061005 (2019).
⁷ K. Tanahashi, S. Takayanagi, T. Motohashi, and S. Tanaka, J. Phys. Soc. Jpn. **88**, 061010 (2019).
⁸ H. Mukai, A. Tomonaga, and J.-S. Tsai, J. Phys. Soc. Jpn. **88**, 061011 (2019).
⁹ M. Maezawa, *et al.*, J. Phys. Soc. Jpn. **88**, 061012 (2019).
¹⁰ V. Karanikolas, and S. Kawabata, J. Phys. Soc. Jpn. **89**, 094003 (2020).
¹¹ A.D. King, *et al.*, Nature **560**, 456 (2018).
¹² M. W. Johnson, *et al.*, Nature **473**, 194 (2011).
¹³ A. Lucas, Front. Phys., **2**, 5 (2014).
¹⁴ V. Choi, Quant. Inf. Proc. **7**, 193 (2008).
¹⁵ V. Choi, Quant. Inf. Proc. **10**, 343 (2011).
¹⁶ W. Lechner, P. Hauke, and P. Zoller, interactions, Sci. Adv. **1**, e1500838 (2015).
¹⁷ T. Albash, W. Vinci, and D. A. Lidar, Phys. Rev. A **94**, 022327 (2016).
¹⁸ T. Onodera, E. Ng and P. L. McMahon, npj Quantum Inf. **6**, 48 (2020).
¹⁹ H. Goto, J. Phys. Soc. Jpn **88**, 061015 (2019).
²⁰ S.E. Nigg, N. Lörch, and R.P. Tiwari, Sci. Adv. **3**, e1602273 (2017).
²¹ S. Puri, C.K. Andersen, A.L. Grimsmo, and A. Blais, Nat. Commun. **8**, 15785 (2017).
²² T. Tanamoto, Phys. Rev. A **88** 062334 (2013).
²³ W. Lechner, arXiv preprint, arXiv:1802.01157.
²⁴ E. Farhi, J. Goldstone, and S. Gutmann, arXiv preprint arXiv:1411.4028 (2014).
²⁵ M. Leib, P. Zoller, and W. Lechner, Quantum Science and Technology **1**, 015008 (2016).
²⁶ N. Schuch and J. Siewert, Phys. Rev. A **67**, 032301 (2003).
²⁷ R. Kosloff and H. Tal-Ezer, Chem. Phys. Lett. **127**, 223 (1986).
²⁸ T. Tanamoto, Y. Nishi, and J. Deguchi, J. Phys. Soc. Jpn. **88**, 061013 (2019).
²⁹ T. Tanamoto, Y. Higashi, and J. Deguchi, J. Appl. Phys. **124**, 154301 (2018).